Discrete Comput Geom (2018) 60:9–26
https://doi.org/10.1007/s00454-017-9928-1

Ma–Schlenker *c*-Octahedra in the 2-Sphere

John C. Bowers[1] · **Philip L. Bowers**[2]

Received: 6 July 2016 / Revised: 28 July 2017 / Accepted: 26 August 2017 /
Published online: 7 September 2017

Abstract We present constructions inspired by the Ma–Schlenker example of "Non-rigidity of spherical inversive distance circle packings" (Discrete Comput Geom 47(3):610–617, 2012). In contrast to the use in Ma and Schlenker (2012) of an infinitesimally flexible Euclidean polyhedron, embeddings in de Sitter space, and Pogorelov maps, our elementary constructions use only the inversive geometry of the 2-sphere.

Keywords Inversive geometry · Circle packing · Circle octahedra

Mathematics Subject Classification 52C26

Introduction

In [2], Bowers and Stephenson questioned whether inversive distance circle packings of surfaces are uniquely determined by their underlying triangulation and the inversive distances between the pairs of adjacent circles. Guo [3] confirmed the local rigidity of inversive distance circle packings on closed orientable surfaces of positive genus, and subsequently Luo [4] verified the global rigidity of these packings, answering

Editor in Charge: Kenneth Clarkson

John C. Bowers
bowersjc@jmu.edu

Philip L. Bowers
bowers@math.fsu.edu

[1] Department of Computer Science, James Madison University, Harrisonburg, VA 22806, USA

[2] Department of Mathematics, The Florida State University, Tallahassee, FL 32306, USA

the Bowers–Stephenson question in the affirmative. Contrasted to this is the beautiful and surprising example of Ma and Schlenker in [5] that provides a counterexample to uniqueness in the spherical case. They produced pairs of packing radii that determine pairs of geodesic triangulations and circle packings on the 2-sphere $\mathbb{S}^2$ realizing the same inversive distance data, but for which there is no inversive transformation taking one of the circle patterns to the other. This was doubly surprising as the famous Koebe–Andre'ev–Thurston Circle Packing Theorem implies uniqueness of spherical packings up to inversive equivalence whenever the edge labels are all in the unit interval—the case of tangent or overlapping circle packings.

The ingredients of Ma and Schlenker's example are Schönhardt's twisted octahedron (an infinitesimally flexible polyhedron in Euclidean space $\mathbb{E}^3$), embeddings in de Sitter space $\mathbb{S}^3_1$, and special properties of the Pogorelov map between different geometries. In contrast, we provide a construction of a large family of Ma–Schlenker-like examples using only inversive geometry. In fact, we show how to construct many counterexamples to the uniqueness of inversive distance circle packings in the 2-sphere.

1 Preliminaries from Circle Packing and Inversive Geometry

1.1 Inversive Distance in the Plane and the 2-Sphere

Let C_1 and C_2 be distinct circles in the complex plane $\mathbb{C}$ centered at the respective points p_1 and p_2, of respective radii r_1 and r_2, and bounding the respective *companion disks* D_1 and D_2. The *inversive distance* $\langle C_1, C_2\rangle$ between C_1 and C_2 is

$$\langle C_1, C_2\rangle = \frac{|p_1 - p_2|^2 - r_1^2 - r_2^2}{2r_1r_2}. \tag{1.1}$$

The *absolute inversive distance* between distinct circles is the absolute value of the inversive distance and is a Möbius invariant of the placement of two circles in the plane. The important geometric facts that make the inversive distance useful in inversive geometry and circle packing are as follows. When $\langle C_1, C_2\rangle > 1$, $D_1 \cap D_2 = \emptyset$ and $\langle C_1, C_2\rangle = \cosh\delta$, where δ is the hyperbolic distance between the totally geodesic hyperbolic planes in the upper-half-space model $\mathbb{C}\times(0,\infty)$ of $\mathbb{H}^3$ whose ideal boundaries are C_1 and C_2. When $\langle C_1, C_2\rangle = 1$, D_1 and D_2 are tangent at their single point of intersection. When $1 > \langle C_1, C_2\rangle \geq 0$, D_1 and D_2 overlap with angle $0 < \theta \leq \pi/2$ with $\langle C_1, C_2\rangle = \cos\theta$. In particular, $\langle C_1, C_2\rangle = 0$ precisely when $\theta = \pi/2$. We shall have no need to use the case when $\langle C_1, C_2\rangle < 0$, when D_1 and D_2 overlap by an angle greater than $\pi/2$.

In the 2-sphere $\mathbb{S}^2$, the inversive distance may be expressed as[1]

$$\langle C_1, C_2\rangle = \frac{-\cos\sphericalangle(p_1, p_2) + \cos(r_1)\cos(r_2)}{\sin(r_1)\sin(r_2)}. \tag{1.2}$$

[1] In both Luo [4] and Ma–Schlenker [5] there is a typo in the expression for the spherical formula for inversive distance. They report the negative of this formula. A quick 2nd order Taylor approximation shows that this formula reduces to Expression (1.1) in the limit as the arguments of the sines and cosines approach zero.

Here, $\sphericalangle(p_1, p_2)$ denotes the spherical distance between the centers, p_1 and p_2, of the respective circles[2] C_1 and C_2 with respective spherical radii r_1 and r_2.[3] Stereographic projection to the plane $\mathbb{C}$ preserves the absolute inversive distance of circle pairs and, as long as neither of the two companion disks D_1 and D_2 contains the north pole, it preserves the inversive distance.

1.2 Edge-Labeled Triangulations of the 2-Sphere and Inversive Distance Circle Packings

We are concerned here with configurations of circles in the 2-sphere $\mathbb{S}^2$ with a specified pattern of inversive distances. Let K be an abstract oriented triangulation of $\mathbb{S}^2$ and $\beta\colon E(K) \to \mathbb{R}$ a mapping defined on $E(K)$, the set of edges of K. Call K together with β an *edge-labeled triangulation* with *edge label* β and denote it as K_β. We denote an edge of K with vertices u and v by uv, and an oriented face with vertices u, v, and w ordered respecting the orientation of K by uvw.

Definition 1.1 A *circle realization* for K_β is a collection $\mathcal{C} = \{C_v : v \in V(K)\}$ of circles in either the plane $\mathbb{C}$ or the 2-sphere $\mathbb{S}^2$ indexed by the vertex set $V(K)$ of K such that $\langle C_u, C_v\rangle = \beta(uv)$ whenever uv is an edge of K. When uv is an edge of K, the corresponding circles C_u and C_v are said to be *adjacent*.

An *inversive distance circle packing for* K_β, or *circle packing* for short, is a circle realization in the 2-sphere where the circles are placed in a way that the circles C_u, C_v, and C_w form a positively oriented triple in $\mathbb{S}^2$ whenever uvw is a positively oriented face of K. We will confine our interest to a restricted class of circle packings, those circle packings that are produced by the use of polyhedral metrics, as presented by Ma and Schlenker in their construction. These are precisely those circle realizations that produce isomorphic copies of the triangulation K by connecting the centers of adjacent circles by geodesic segments. We warn the reader, though, that when β may take values greater than unity so that adjacent circles are separated, this property of a geodesic triangulation in the pattern of K appearing when connecting centers in general is not preserved by Möbius transformations.

1.3 Möbius Flows

The most important ingredients from inversive geometry needed to construct our examples are the Möbius flows associated to two distinct circles in the extended complex plane. Here are the pertinent facts. Circles $C_1 \neq C_2$ lie in a unique *coaxial family*

[2] Any circle in $\mathbb{S}^2$ bounds two distinct disks. Without explicitly stating so, we always assume that one of these has been chosen as a companion disk. The center and radius of a circle in $\mathbb{S}^2$ are the center and radius of its companion disk. The ambiguity should cause no confusion.

[3] It is in no way obvious that formulæ (1.1) and (1.2) are Möbius invariants of circle pairs. There is a not so well-known development of inversive distance, which applies equally in spherical, Euclidean, and hyperbolic geometry, that uses the cross-ratio of the four points of intersection of C_1 and C_2 with a common orthogonal circle. It is computationally less friendly than (1.1) and (1.2), but has the theoretical advantage of being manifestly Möbius-invariant. See [1].

$\mathcal{A}_{C_1,C_2}$ of circles in the extended complex plane $\widehat{\mathbb{C}}$ whose elements serve as the flow lines of certain 1-parameter subgroups of the Möbius group $\text{Möb}(\widehat{\mathbb{C}}) \cong \text{PSL}(2,\mathbb{C})$ acting on the extended plane as linear fractional transformations. The family $\mathcal{A}_{C_1,C_2}$ is invariant under these flows. When C_1 and C_2 are disjoint, any such flow is an *elliptic flow* conjugate in $\text{Möb}(\widehat{\mathbb{C}})$ to a standard rotation flow of the form $t \mapsto R_{\lambda t}$, where $\lambda \neq 0$ and $R_{\lambda t}$ is the rotation $z \mapsto e^{\lambda i t} z$. When C_1 and C_2 meet in a single point p, the flow is *parabolic* and is conjugate in $\text{Möb}(\widehat{\mathbb{C}})$ to a standard translation flow of the form $t \mapsto T_{\lambda t}$, where $\lambda \neq 0$ and $T_{\lambda t}$ is the translation $z \mapsto z + \lambda t$. Finally, when C_1 and C_2 meet in two distinct points a and b, the flow is *hyperbolic* and is conjugate in $\text{Möb}(\widehat{\mathbb{C}})$ to a standard scaling flow of the form $t \mapsto S_{\lambda t}$, where $\lambda \neq 0$ and $S_{\lambda t}$ is the scaling map $z \mapsto e^{\lambda t} z$. All the flows determined by two fixed circles C_1 and C_2 are said to be *equivalent flows*, with two such flows differing only in the value of the parameter λ, with $|\lambda|$ the *speed* of the flow. Note that any two distinct circles in the coaxial family $\mathcal{A}_{C_1,C_2}$ determine the same Möbius flows as C_1 and C_2. Of course, any Möbius flow preserves the inversive distances between circles.

Each coaxial family $\mathcal{A}$ has an associated *orthogonal complement* $\mathcal{A}^\perp$, this also a coaxial family for which each circle of $\mathcal{A}$ is orthogonal to each circle of $\mathcal{A}^\perp$. In fact, $\mathcal{A}^\perp$ is exactly the collection of circles (and lines) that are orthogonal to every member of $\mathcal{A}$, and of course $\mathcal{A}^{\perp\perp} = \mathcal{A}$. Any flow whose flow lines are the circles of $\mathcal{A}$ is generated by inversions through the circles of the orthogonal complement $\mathcal{A}^\perp$.

2 Ma–Schlenker *c*-Octahedra: The Examples Writ Large

In this section we detail examples of pairs of spherical circle packings for a fixed edge-labeled triangulation that fail to be inversive equivalent. These were discovered by studying the properties of the first family of such examples constructed by Ma and Schlenker in [5] using fairly sophisticated geometric constructions. Ours are constructed using Möbius flows and, having properties reminiscent of the Ma–Schlenker examples, will be named after them. This section presents a general construction of such examples and describes their important properties, and the next verifies the claimed properties.

Let $\mathcal{O}$ be the octahedral triangulation of the 2-sphere with six vertices, each of valence four, twelve edges, and eight faces, and combinatorially equivalent to the boundary of a regular octahedron. The 1-skeleton graph of $\mathcal{O}$ is shown embedded in the plane in Fig. 1(a).

Definition 2.1 The edge-labeled triangulation $\mathcal{O}_\beta$ is called a *Ma–Schlenker octahedron* provided β takes a constant value $a \geq 0$ on the edges of a fixed face uvw, a constant value $d \geq 0$ on the edges of its opposite face $w'v'u'$, and alternates between the values $b \geq 0$ and $c \geq 0$ on the 'teepee' of edges connecting the vertices of these two opposite faces, as in Fig. 2. When we need to emphasize the values of a, b, c, and d, we denote $\mathcal{O}_\beta$ as $\mathcal{O}(a,b,c,d)$.

Definition 2.2 A circle packing for a Ma–Schlenker octahedron is called a *Ma–Schlenker circle-octahedron*, or a *Ma–Schlenker c-octahedron* for short. A pair of

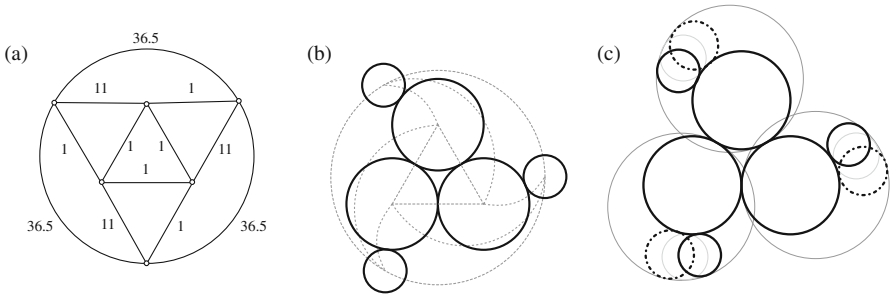

Fig. 1 A critical Ma–Schlenker circle octahedron and two non-inversive equivalent nearby patterns with the same inversive distances on the graph. (a) Octahedral graph labeled with the inversive distances from (b). (b) A planar circle pattern realizing the octahedral graph in (a). (c) Two non-equivalent realizations with inversive distance 37 on the outer edges

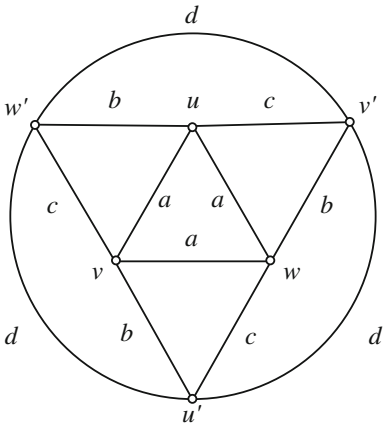

Fig. 2 The typical Ma–Schlenker octahedron $\mathcal{O}(a, b, c, d)$

circle packings, $\mathcal{C}$ and $\mathcal{C}'$, for the same Ma–Schlenker octahedron $\mathcal{O}_\beta$ is called a *Ma–Schlenker pair* provided $\mathcal{C}$ and $\mathcal{C}'$ are not inversive equivalent.

2.1 The Construction

We now describe a method for constructing Ma–Schlenker pairs. It begins with a construction of a 1-parameter family of planar circle realizations of Ma–Schlenker octahedra $\mathcal{O}(a, b, c, d(t))$ where a, b, and c are fixed while $d = d(t)$ varies. Figure 3 presents a graphical description of this construction in a special case. Fix a non-negative number a and choose three circles C_u, C_v, and C_w in the complex plane that are centered at the respective vertices of an equilateral triangle Δ so that $\langle C_u, C_v\rangle = \langle C_v, C_w\rangle = \langle C_w, C_u\rangle = a$. Normalize by insisting that Δ have side length 2 with circle C_u centered on $z = -1$, C_v centered on $z = 1$, and C_w centered on $z = \boldsymbol{i}\sqrt{3}$, placing the incenter of Δ at $z = \boldsymbol{i}/\sqrt{3}$. Let $\mathcal{A} = \mathcal{A}_{C_u,C_v}$ be the coaxial family containing C_u and C_v and note that the line of centers of $\mathcal{A}$ is the real axis $\mathbb{R}$ and the radical axis of $\mathcal{A}$ is the imaginary axis $\mathbb{R}\boldsymbol{i}$. Choose an *initial circle* C centered

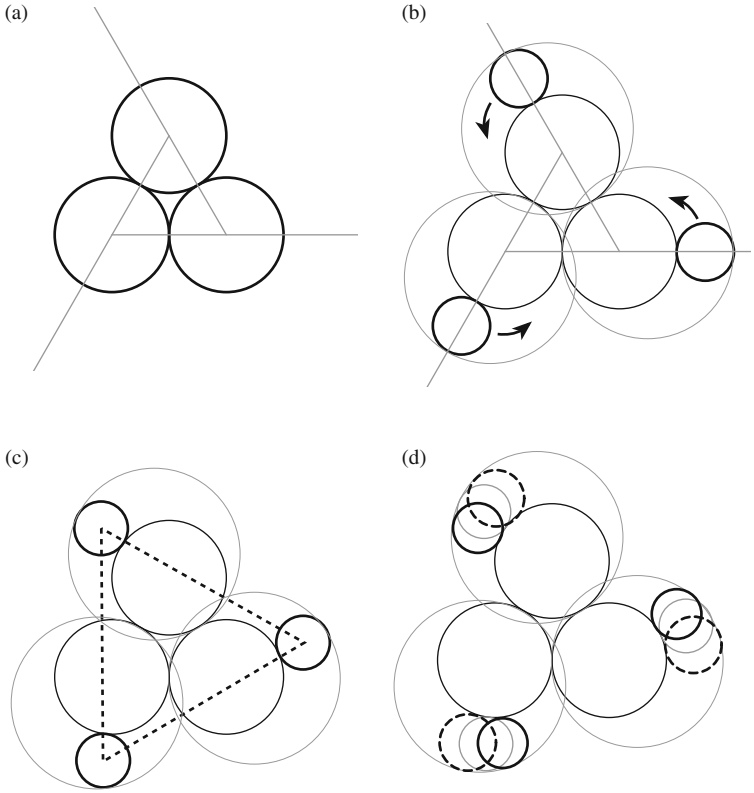

Fig. 3 The construction for a particular Ma–Schlenker pair. (a) Start with three *circles* of equal radii centered at the vertices of an equilateral *triangle*. Extend rays in order around the edges. (b) Take three *circles* of equal radii at a fixed distance along each ray to form the outer face. (c) Flow the *outer circles* symmetrically until the inversive distance reaches a minimum value. This is the critical *circle* realization. (d) Flow to find a pair of circle realizations (*solid* and *dashed*) near the critical packing that have equal inversive distances on the outer face. These are not Möbius equivalent

on the positive real axis such that $c = \langle C_v, C\rangle \geq 0$ and let $b = \langle C_u, C\rangle$. Note that $b > c$. Let $\mu = \{\mu_t : t \in \mathbb{R}\}$ be the unit speed Möbius flow determined by $\mathcal{A}$ that is counterclockwise on the circle C_v, and let $1 < x_1 < x_2$ be the points of intersection of C with the real axis. Let $A_1, A_2 \in \mathcal{A}$ be the circles in the family $\mathcal{A}$ containing x_1 and x_2, respectively. For any real number t, $\mu_t(C)$ is a circle tangent to both A_1 and A_2 and sits between them, external to the disk bounded by A_1 and internal to the disk bounded by A_2. See Fig. 4 for illustrations of the family $\{\mu_t(C) : t \in \mathbb{R}\}$ when the flow is hyperbolic ($0 \leq a < 1$), parabolic ($a = 1$), and elliptic ($a > 1$). Since the flow μ preserves the individual circles of the coaxial system $\mathcal{A}$, $\langle C_u, \mu_t(C)\rangle = b$ and $\langle C_v, \mu_t(C)\rangle = c$ for all $t \in \mathbb{R}$.

Let $\mathfrak{r}$ be the counterclockwise rotation of the plane $\mathbb{C}$ through angle $2\pi/3$ with fixed point $\boldsymbol{i}/\sqrt{3}$, the incenter of the triangle Δ. The circle configuration $\mathcal{C}(t)$ is defined as the collection

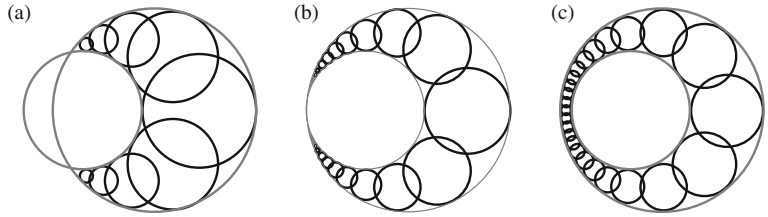

Fig. 4 Möbius flows from the construction. The *smaller gray circle* is A_1 and the larger is A_2. (a) Hyperbolic ($0 \leq a < 1$). (b) Parabolic ($a = 1$). (c) Elliptic ($a > 1$)

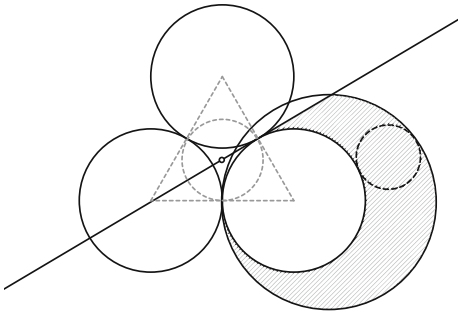

Fig. 5 The center of the critical *circle* must fall within the *shaded* region

$$\mathcal{C}(t) = \left\{C_u, C_v, C_w, C_{w'}(t) = \mu_t(C), C_{u'}(t) = \mathfrak{r}(\mu_t(C)), C_{v'}(t) = \mathfrak{r}^2(\mu_t(C))\right\}. \tag{2.1}$$

The properties of $\mathcal{C}(t)$ of interest to us are, first, for all $t \in \mathbb{R}$ the configuration $\mathcal{C}(t)$ of circles in the plane is a circle realization for the Ma–Schlenker octahedron $\mathcal{O}(a, b, c, d(t))$, where

$$d(t) = \langle \mu_t(C), \mathfrak{r}(\mu_t(C)) \rangle, \tag{2.2}$$

and second, for all $t \in \mathbb{R}$, $\mathcal{C}(t)$ has order three rotational symmetry about the incenter of Δ via the rotation $\mathfrak{r}$. Stereographic projection of $\mathcal{C}(t)$ to $\mathbb{S}^2$ defines a 1-parameter family of circle realizations for $\mathcal{O}(a, b, c, d(t))$ in the 2-sphere, though these are not a priori circle packings. These realizations possibly must be repositioned to a normalized position by applying Möbius transformations of $\mathbb{S}^2$ to find appropriate intervals of t-values that produce the desired circle packings.

Our goal is to find values of the inversive distance parameters $a > 1/2$ and $b > c \geq 0$ so that the function $d(t)$ has a critical value at a parameter value $t = \tau$, with $d(\tau)$ a local minimum for d, and for which the circle $\mu_\tau(C)$ is centered in the interior of the closed half-plane H containing $z = 1$, the center of C_v, and bordered by the line through $z = -1$, the center of C_u, and the incenter of Δ; see Fig. 5. *Moreover, $\mu_\tau(C)$ should have positive inversive distance to the unique circle O orthogonal to C_u, C_v, and C_w. The circle O exists since $a > 1/2$. The claim is that with these conditions satisfied, Ma–Schlenker pairs may be produced.*

To see this, let O' be the unique circle orthogonal to $C_{u'}(\tau)$, $C_{v'}(\tau)$, and $C_{w'}(\tau)$, which exists since $d(\tau) > 1/2$.[4] By the order three rotational symmetry of $\mathcal{C}(t)$, O and O' are concentric, both centered at $\boldsymbol{i}/\sqrt{3}$. Let $\widetilde{\mathcal{C}}(t)$ be the image of $\mathcal{C}(t)$ under stereographic projection to the 2-sphere followed by a Möbius transformation so that (1) the respective images of the circles O and O' are latitudinal circles, the first centered on the south pole and contained in the southern hemisphere, and the second on the north pole and contained in the northern hemisphere, and (2) the circles L and L' have the same radius, L centered on the south pole and L' on the north, where L is the latitudinal circle containing the centers of the projections of C_u, C_v, and C_w, and L' is the latitudinal circle containing the centers of the projections of $C_{u'}(\tau)$, $C_{v'}(\tau)$, and $C_{w'}(\tau)$. Note that the order three rotational symmetry of $\mathcal{C}(t)$ translates to an order three rotational symmetry of $\widetilde{\mathcal{C}}(t)$ by a rotation of $\mathbb{S}^2$ about the axis through the north and south poles.

Our claim is that there is an open interval J of t-values containing τ for which each $\widetilde{\mathcal{C}}(t)$, for $t \in J$, is a circle packing. Since then the Ma–Schlenker c-octahedron $\widetilde{\mathcal{C}}(\tau)$ provides a minimum value for $d(t)$, variation of t about τ produces (possibly with further restrictions on a, b, and c) pairs $t < \tau$ and $t' > \tau$ in J for which $\widetilde{\mathcal{C}}(t)$ and $\widetilde{\mathcal{C}}(t')$ form a Ma–Schlenker pair, two circle packings for $\mathcal{O}(a, b, c, d)$, where $d = d(t) = d(t')$, that fail to be inversive equivalent.

Definition 2.3 The circle realization $\mathcal{C}(\tau)$ is said to be *critical*, the circle packing $\widetilde{\mathcal{C}}(\tau)$ is a *critical Ma–Schlenker c-octahedron*, and the corresponding edge-labeled triangulation $\mathcal{O}(a, b, c, d(\tau))$ is a *critical Ma–Schlenker octahedron*. See Fig. 6 for a 3D visualization of a critical Ma–Schlenker c-octahedron.

The claim of the preceding paragraph, that there is an open interval J of t-values containing τ for which each $\widetilde{\mathcal{C}}(t)$, for $t \in J$, is a circle packing follows from the fact that the circle $\mu_\tau(C)$ is centered in the interior of the closed half-plane H. The point is that three points u, v, and w equally spaced on L and u', v' and w' equally spaced on L' with u and w' on the same meridian, v and u' on the same meridian, and w and v' on the same meridian, cut out an octahedral triangulation of $\mathbb{S}^2$ when points are connected according to the Ma–Schlenker octahedral pattern. Assuming the points are ordered counterclockwise when viewed from the north pole, if now the points along L' are rotated counterclockwise by an angle strictly between 0 and π, then this triangulation "stretches" to form a triangulation with vertices u, v, and w, and the rotated u', v', and w'. It is only when the rotation reaches π radians that there is ambiguity as then u and w' are antipodal, and then as w' is rotated past π radians, the geodesic arc connecting u to w' moves to the other side of the north pole, and the triangle uvw' now contains the north pole, as do vwu' and wuv'. At this point we have lost the triangulation. The point of the half-plane is that the center of $\mu_\tau(C)$ in the interior of H guarantees that the position of w' is obtained in this manner by a positive counterclockwise rotation strictly less than π.

We have used the restriction $a > 1/2$ to ensure the existence of a circle mutually orthogonal to the three circles C_u, C_v, and C_w. This in turn is used to ensure that stereographic projection followed by an appropriate Möbius transformation produces, not just a realization, but a circle packing for a Ma–Schlenker octahedron. This is done

[4] By an application of (3.14).

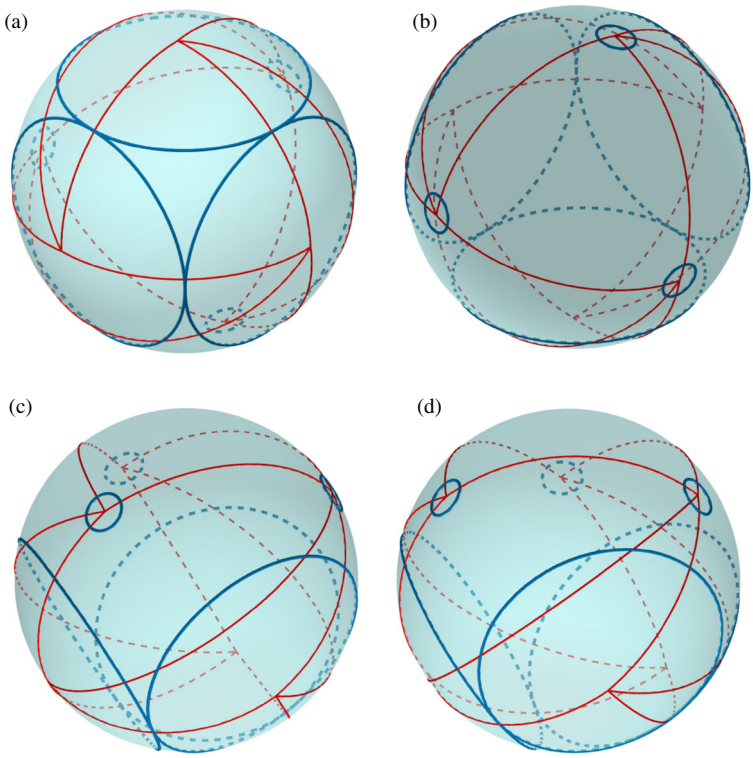

Fig. 6 A 3D visualization of a critical Ma–Schlenker octahedron showing the triangulation. (a) A view from the south pole. (b) A view from the north pole. (c) A view from slightly north of the equator. (d) A slight rotation from (c)

for convenience of argument and we mention that even if $a \leq 1/2$, when there is no mutually orthogonal circle to C_u, C_v, and C_w, Ma–Schlenker circle packings are still possible.

3 Ma–Schlenker c-Octahedra: The Devil of the Details

Figures 7, 8 and 9 show examples of the graphs of $d(t)$ for various values of a and choices of initial circle C. The Ma–Schlenker pairs arise from pairs t and t' near τ and at the same horizontal level on the graph of $d(t)$. A precise description of the derivation of these graphs is given subsequently, after we make some observations.

3.1 The Parabolic Case

Here $a = 1$, the circles C_u, C_v and C_w are mutually tangent, and the flow is parabolic. An example is shown in Fig. 7(a), where the initial circle C meets the real axis at $x_1 = 1.7$ and $x_2 = 3$, with $b = \langle C_u, C\rangle = 7.538$ and $c = \langle C_v, C\rangle = 0.308$.

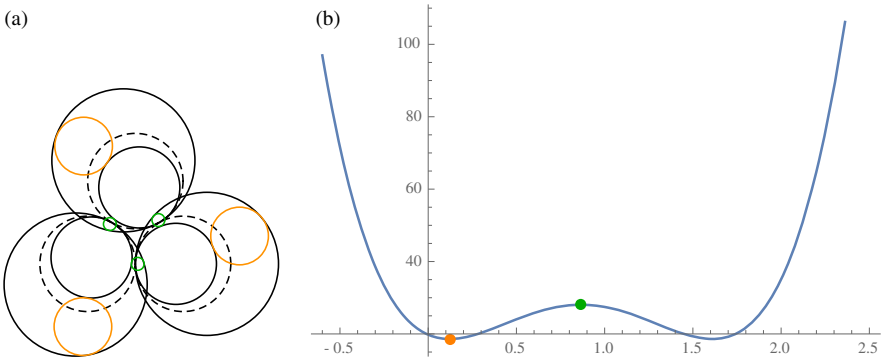

Fig. 7 A parabolic flow. The parameters are $x_1 = 1.7$, $x_2 = 3$. The highlighted minimum and (local) maximum occur at $\tau = t_{\min} = 0.121766$ (*orange*) and $m = t_{\max} = 0.866025$ (*green*), and the inversive distances are $d(t_{\min}) = 18.6065$ and $d(t_{\max}) = 28.051$ (computed values are rounded). (a) Parabolic flow. (b) Graph of the inversive distance function $d(t)$

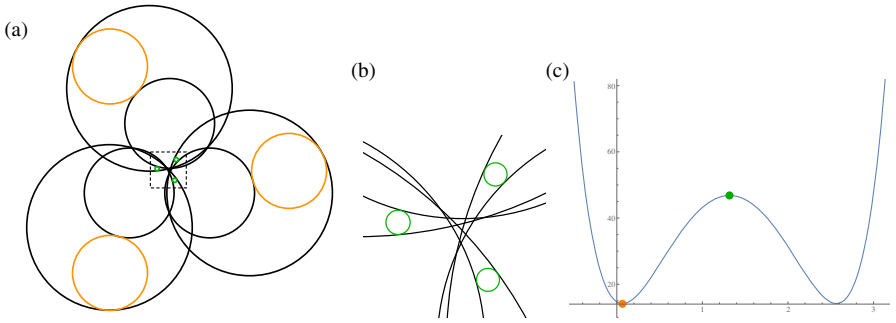

Fig. 8 Hyperbolic flow. The parameters are $x_1 = 2.11803$, $x_2 = 4.06155$, and $y = 0.5$. The highlighted minimum (*orange*) occurs at $\tau = t_{\min} = 0.06782$ and the local maximum (*green*) at $m = t_{\max} = 1.31696$. The inversive distances are $d(t_{\min}) = 14.1647$ and $d(t_{\max}) = 46.8136$. (a) Hyperbolic flow. (b) Detail of the *dotted box*. (c) Graph of the inversive distance

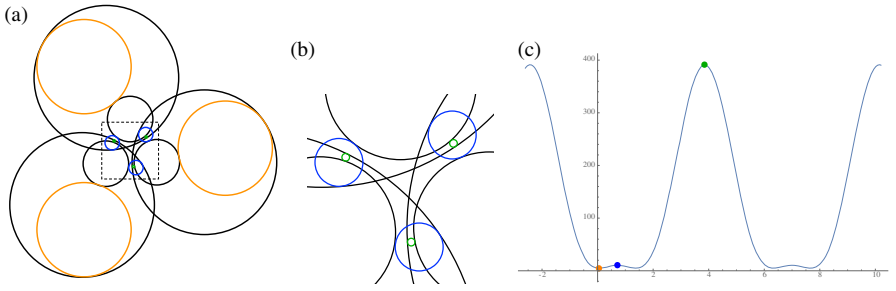

Fig. 9 An elliptic flow. The parameters are $x_1 = 2$, $x_2 = 6$, and $y = 0.5$. The highlighted minimum (*orange*) occurs at $\tau = t_{\min} = 0.0506$, the local maximum (*blue*) at $m = t^{(1)}_{\max} = 0.7137$, and the absolute maximum (*green*) at $M = t^{(2)}_{\max} = 3.85532$. The inversive distances are $d(t_{\min}) = 5.000$, $d(t^{(1)}_{\max}) = 10.4245$, and $d(t^{(2)}_{\max}) = 391.247$. (a) Elliptic flow. (b) Detail of the *dotted box*. (c) Graph of the inversive distance, which is periodic of period 2π

The three circles C_u, C_v and C_w are the dotted circles. The critical circle $C(\tau)$, in orange, gives a minimum value for $d(t)$ and is centered in the half-plane H. The graph of $d(t)$ is shown in Fig. 7(b), whose shape is typical of all the examples with $a = 1$. The general characteristics of the parabolic flow are the same as for the hyperbolic, which is described in detail in the next paragraph.

3.2 The Hyperbolic Case

Here $1/2 < a \leq 1$ and the pairs of circles among C_u, C_v, and C_w meet at angle $\pi/3 \geq \theta = \cos^{-1} a \geq 0$. The center of the unique circle O orthogonal to C_u, C_v and C_w is the incenter $\boldsymbol{i}/\sqrt{3}$ of Δ, and lies in the bounded interstice formed by C_u, C_v and C_w. As $t \to \pm\infty$, the inversive distance parameter $d(t) \to +\infty$. The absolute minimum value of $d(t)$ occurs at two distinct t-values $0 < \tau < \tau'$, which implies that both circles, $C(\tau) = \mu_\tau(C)$ and $C(\tau') = \mu_{\tau'}(C)$, are centered in the first quadrant of the complex plane. Between these lies a parameter value m at which $d(t)$ obtains a local maximum. The circle $C(m) = \mu_m(C)$ is orthogonal to O and inversion I_O through the circle O preserves $C(m)$ and exchanges circles $C(\tau)$ and $C(\tau')$. The center of $C(\tau)$ lies outside of O, and that of $C(\tau')$ inside. More generally, the inversion I_O generates a symmetry of the graph in the following way. Since O is in the orthogonal complement $\mathcal{A}^{\perp}_{C_u,C_v}$, the inversion I_O preserves the family $\mathcal{A} = \mathcal{A}_{C_u,C_v}$, merely inverting each circle of $\mathcal{A}$ to itself. In particular, since A_1 and A_2 are members of $\mathcal{A}$ and form the envelope of the family $\mathcal{B} = \{\mu_t(C) : t \in \mathbb{R}\}$ of circles generated by the Möbius flow μ, $I_O(A_1) = A_1$ and $I_O(A_2) = A_2$ form the envelope of the circles of the family $I_O(\mathcal{B})$, implying that I_O preserves the family $\mathcal{B}$. It follows that I_O generates an involution of $\mathbb{R}$. Indeed, for each $t \in \mathbb{R}$, let t' be the real value for which $\mu_{t'}(C) = I_O(\mu_t(C))$. Then $t'' = t$ with fixed point $m = m'$. This generates a symmetry of the graph of $d(t)$ with $d(t) = d(t')$ since

$$\begin{aligned} d(t) &= \langle \mu_t(C), \mathfrak{r}(\mu_t(C)) \rangle \\ &= \langle I_O(\mu_t(C)), I_O(\mathfrak{r}(\mu_t(C))) \rangle \\ &= \langle I_O(\mu_t(C)), \mathfrak{r}(I_O(\mu_t(C))) \rangle \\ &= \langle \mu_{t'}(C), \mathfrak{r}(\mu_{t'}(C)) \rangle = d(t'), \end{aligned}$$

since the inversion I_O commutes with the rotation $\mathfrak{r}$, as both are centered at $\boldsymbol{i}/\sqrt{3}$.

Figure 8 presents an example where $a = 0.6$ with the angle θ of intersection of C_u and C_v equal to $2\tan^{-1}(1/2) \cong 0.9273$. The three circles C_u, C_v and C_w are suppressed in the figure, and the respective values of b and c are $b = 6.689$ and $c = 1$. The circles C_u and C_v meet at $\pm y\boldsymbol{i}$ where $y = 0.5$. In the close up of Fig. 8(b), the three local maximum circles (green) and the six enveloping circles are orthogonal to O (not shown).

3.3 The Elliptic Case

Here $a > 1$ and the facts are similar to those of the hyperbolic case. The primary difference is that $d(t)$ now is periodic of period $\omega = 2\pi/|\lambda|$, where $|\lambda|$ is the speed

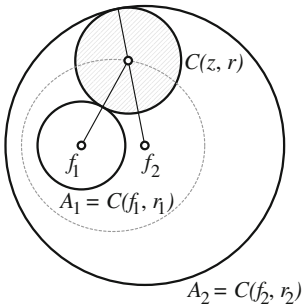

Fig. 10 The centers of $C(z, r)$ lie on the *dotted ellipse* with equation $|z - f_1| + |z - f_2| = r_1 + r_2$

of the elliptic flow. There are parameter values $0 < \tau < m < \tau' < M < \omega$ where $d(\tau) = d(\tau')$ is the absolute minimum value, $d(m)$ is a local maximum value, and $d(M)$ is the absolute maximum value. The circles $C(m) = \mu_m(C)$ and $C(M) = \mu_M(C)$ are orthogonal to O and $C(\tau) = \mu_\tau(C)$ and $C(\tau') = \mu_{\tau'}(C)$ are centered in the first quadrant and are exchanged by the inversion I_O, which generates a periodic symmetry of the graph similar to the case articulated in the preceding paragraph.

Figure 9 presents an example where $a = 5/3$ and the coaxial family $\mathcal{A}$ has foci $\pm y$, where $y = 0.5$. The three circles C_u, C_v and C_w are suppressed in the figure, and the respective values of b and c are $b = 5.846$ and $c = 1.227$. In the close up of Fig. 9(b), the three local maximum circles (blue), the three absolute maximum circles (green), and the six enveloping circles are orthogonal to O (not shown).

3.4 Formulæ

The next order of business is to derive useful formulæ for analyzing $d(t)$. Let $C(z, r)$ denote the circle in the complex plane centered at z and of radius $r > 0$. The inversive distance between the circle $C(z, r)$ and its rotated cousin $\mathfrak{r}(C(z, r)) = C(\mathfrak{r}(z), r)$ is

$$h(z, r) = \frac{|z - \mathfrak{r}(z)|^2 - 2r^2}{2r^2} = \frac{1}{2}\,\frac{|\sqrt{3}z - \boldsymbol{i}|^2}{r^2} - 1. \tag{3.1}$$

Let f_1 and f_2 be the respective centers of the two circles A_1 and A_2. A glance at Fig. 10 should convince the reader that if $C(z, r)$ is externally tangent to A_1 and internally tangent to A_2, then $|z - f_1| = r_1 + r$ and $|z - f_2| = r_2 - r$, where r_1 and r_2 are the respective radii of the circles A_1 and A_2. It follows that

$$|z - f_1| + |z - f_2| = r_1 + r_2, \tag{3.2}$$

implying that the centers $z = z(t)$ of the circles $\mu_t(C)$ lie on the ellipse described by (3.2). Using $|z - f_1| = r_1 + r$ to eliminate r from (3.1) gives the formula

$$h(z) = \frac{1}{2}\,\frac{|\sqrt{3}z - \boldsymbol{i}|^2}{\big(|z - f_1| - r_1\big)^2} - 1 \tag{3.3}$$

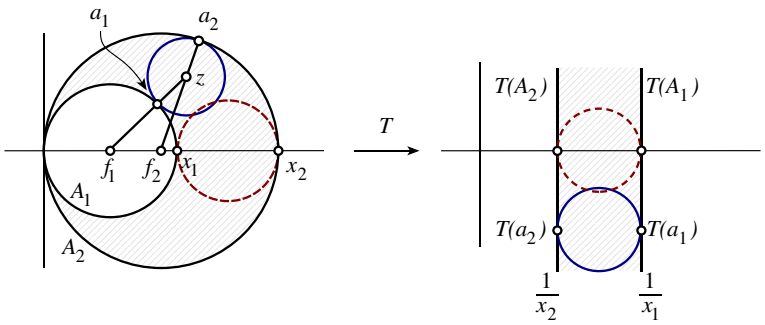

Fig. 11 The canonical Möbius flow for the parabolic case

for the inversive distance between a circle $C(z, r)$ externally tangent to A_1 and its rotated cousin $\mathfrak{r}(C(z, r))$. To find the extrema of the inversive distance function $d(t)$ of (2.2), we need to find the extrema of $h(z)$ of (3.3) when z is subject to the constraint of (3.2).

The ellipse of (3.2) has foci f_1 and f_2 with center $(f_1 + f_2)/2$, major radius $(r_1 + r_2)/2$, and minor radius $\frac{1}{2}\sqrt{(r_1 + r_2)^2 - (f_2 - f_1)^2}$. The Cartesian equation for this ellipse is

$$\frac{(2x - f_1 - f_2)^2}{(r_1 + r_2)^2} + \frac{4y^2}{(r_1 + r_2)^2 - (f_2 - f_1)^2} = 1. \tag{3.4}$$

Equation (3.3) has been used to compute the value of $d(\tau)$, the critical minimum value of $d(t)$ in the examples presented in this paper, and the values of $d(t) = d(t')$ for the Ma–Schlenker pairs. We now describe the derivations of the plots of Figs. 7, 8 and 9. In each case this is accomplished by mapping via a Möbius transformation to a standard flow, applying the standard flow, and mapping back.

3.4.1 The Parabolic Case, Fig. 7

Let $a_1 = a_1(t)$ and $a_2 = a_2(t)$ be the points of tangency of the circle $C(t) = \mu_t(C)$ with the respective enveloping circles A_1 and A_2, as in Fig. 11. We will derive formulæ for a_1 and a_2 in terms of parameters $1 < x_1 < x_2$ and the variable t and use these to write the center $z(t)$ and radius $r(t)$ of $C(t)$ for use in the function

$$d(t) = h(z(t), r(t)) \tag{3.5}$$

of formula (3.1). The Möbius transformation $T(z) = 1/z$, which is its own inverse, maps A_1 to the vertical line $x = 1/x_1$ and A_2 to the vertical line $x = 1/x_2$. The flow μ_t is obtained by conjugation of the standard unit speed flow $\nu_t(z) = z - t\boldsymbol{i}$ with T. The formulæ for $a_1(t)$ and $a_2(t)$ become

$$a_s = a_s(t) = T\left(\frac{1 - x_s t\boldsymbol{i}}{x_s}\right) = x_s \frac{1 + x_s t\boldsymbol{i}}{1 + x_s^2 t^2} \quad \text{for } s = 1, 2.$$

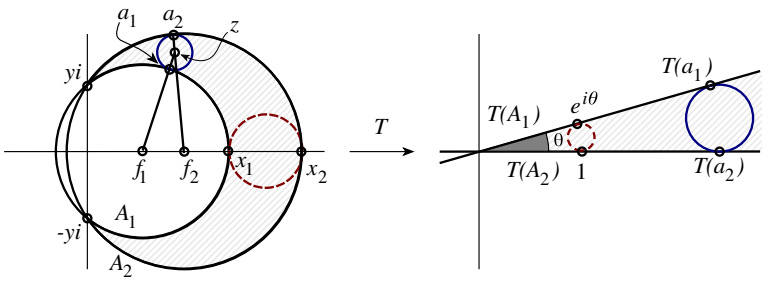

Fig. 12 The canonical Möbius flow for the hyperbolic case

The radius $r(t)$ of $C(t)$ becomes

$$r = r(t) = \frac{r_1 r_2 (a_2(t) - a_1(t))}{r_2(a_1(t) - f_1) + r_1(a_2(t) - f_2)}, \tag{3.6}$$

and its center $z(t)$ becomes

$$z = z(t) = f_1 + (r_1 + r(t)) \frac{a_1(t) - f_1}{r_1}. \tag{3.7}$$

Figure 7 was generated using formulæ (3.6) and (3.7) in (3.5) in `Mathematica`. We have posted `Mathematica` notebooks for generating visualizations of these constructions at https://w3.cs.jmu.edu/bowersjc/page/circles/.

3.4.2 The Hyperbolic Case, Fig. 8

In this case the circles C_u and C_v meet at points $\pm y\boldsymbol{i}$ as in Fig. 12. The relationships among the parameters are that $y < 1/\sqrt{3}$, and for $s = 1, 2$, $f_s^2 + y^2 = r_s^2$ and $x_s = f_s + r_s$. The graphic is computed from (3.5), (3.6), and (3.7) with the only difference from the parabolic case that the formulæ for a_1 and a_2 change. To obtain the correct formulæ, we use the Möbius transformation

$$T(z) = \frac{x_2 - y\boldsymbol{i}}{x_2 + y\boldsymbol{i}} \frac{z + y\boldsymbol{i}}{z - y\boldsymbol{i}} \tag{3.8}$$

to map $-y\boldsymbol{i}$ to 0, $y\boldsymbol{i}$ to ∞, and x_2 to 1. The image of A_2 is the real axis and the image of A_1 is the line through the origin at angle

$$\theta = \cos^{-1}\left(\frac{f_1 f_2 + y^2}{r_1 r_2}\right) \tag{3.9}$$

up from the real axis. The standard unit speed flow is now $v_t(z) = e^t z$ and a_1 and a_2 are given as

$$a_1 = a_1(t) = T^{-1}\left(e^{t+\theta\boldsymbol{i}}\right) \quad \text{and} \quad a_2 = a_2(t) = T^{-1}(e^t), \tag{3.10}$$

Fig. 13 The angle α

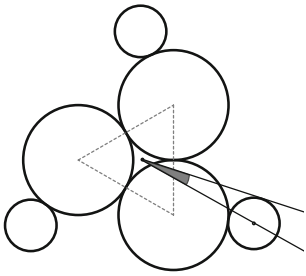

where, setting $\kappa = (x_2 - y\boldsymbol{i})/(x_2 + y\boldsymbol{i})$, we may write T and T^{-1} as

$$T(z) = \kappa\,\frac{z + y\boldsymbol{i}}{z - y\boldsymbol{i}} \quad \text{and} \quad T^{-1}(z) = y\boldsymbol{i}\,\frac{z + \kappa}{z - \kappa}. \tag{3.11}$$

3.4.3 The Elliptic Case, Fig. 9

In this case the circles C_u and C_v are part of a coaxial family with foci $\pm y$. The relationships among the various parameters are $0 < y < 1$, and for $s = 1, 2$, $f_s = (y^2 + x_s^2)/2x_s$ and $r_s = x_s - f_s = (y^2 - x_s^2)/2x_s$. Again, the graphic is computed from (3.5), (3.6), and (3.7) with a_1 and a_2 given by

$$a_1 = a_1(t) = T^{-1}\big(e^{t\boldsymbol{i}}\big) \quad \text{and} \quad a_2 = a_2(t) = T^{-1}\big(e^{t\boldsymbol{i}}T(x_2)\big). \tag{3.12}$$

Here T is the Möbius transformation that takes y to 0, $-y$ to ∞, and x_1 to 1. This takes the circle A_1 to the unit circle and A_2 to a circle centered at the origin of radius greater than 1. The standard unit speed flow is the rotation flow $v_t(z) = e^{t\boldsymbol{i}}z$ and T and T^{-1} are given by

$$T(z) = \kappa\,\frac{z - y}{z + y} \quad \text{and} \quad T^{-1}(z) = -y\,\frac{z + \kappa}{z - \kappa}, \tag{3.13}$$

where $\kappa = (x_1 + y)/(x_1 - y)$.

3.5 The Angular Equation

One more geometric fact is useful. In the setting of the planar construction of Sect. 2.1, let $\alpha = \alpha(t)$ be the angle subtended by the ray from the incenter of the triangle Δ through the center of $C_{w'} = C_{w'}(t)$ and a ray from the incenter that is tangent to $C_{w'}$, as in Fig. 13. It is easy to see that the angle α lies between 0 and $\pi/2$, and an algebraic manipulation determines that

$$d(t) = \langle C_{w'}, \mathfrak{r}(C_{w'})\rangle = \frac{1}{2} + \frac{3}{2}\cot^2\alpha(t). \tag{3.14}$$

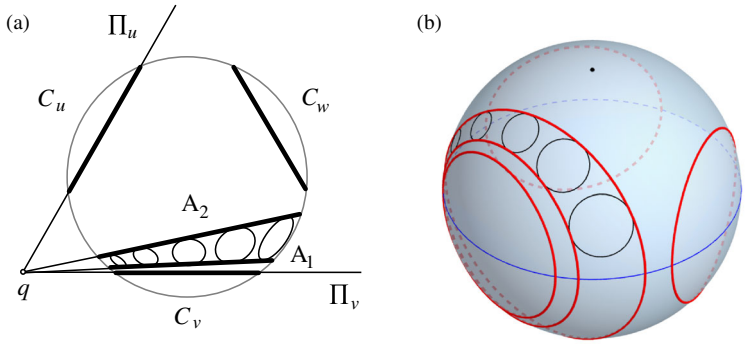

Fig. 14 Two views of a state of the construction of a Ma–Schlenker realization with C_u, C_v, and C_w centered on the equator. (a) Above the north pole. (b) A 3D view

Notice as α strictly increases from 0 to $\pi/2$, the function $\cot^2 \alpha$ strictly decreases from ∞ to 0. Thus the comparison of two values of d may be made simply by comparing the corresponding angles α:

$$d(t) < d(t') \quad \text{if and only if} \quad \alpha(t) > \alpha(t'). \tag{3.15}$$

From this observation one can make quick judgements of the correctness of many of our claims in the examples just by examining the graphics of the planar circle realizations of the figure, perhaps with a straight edge and protractor.

4 The Construction on the Sphere

In this final section we present an alternative description of the construction of Ma–Schlenker realizations, this time directly on the 2-sphere $\mathbb{S}^2$ realized as the unit sphere in $\mathbb{E}^3 = \mathbb{C} \times \mathbb{R}$. In this normalization, the north pole is $\mathsf{n} = (0, 1)$, the south pole is $\mathsf{s} = (0, -1)$, and the equatorial plane is identified with $\mathbb{C}$. The circles C_u, C_v, and C_w in $\mathbb{S}^2$ are of equal radii whose centers are equally spaced on the equator. Projecting orthogonally along the north-south direction to the equatorial plane, the upper hemisphere projects to the unit disk and the three circles C_u, C_v, and C_w project to symmetrically placed chords of the unit circle, as in Fig. 14(a). The orthogonal projections of the typical circles A_1 and A_2 in the coaxial family $\mathcal{A}_{C_u,C_v}$ that form the envelope of the Möbius-flowed circles $C_{w'}(t)$ are shown in Fig. 14(a). The coaxial family $\mathcal{A}_{C_u,C_v}$ is obtained as follows. Let Π_u and Π_v be the 2-planes in $\mathbb{E}^3$ whose respective intersections with the 2-sphere $\mathbb{S}^2$ are the circles C_u and C_v. Let $\ell_{u,v}$ be the line $\Pi_u \cap \Pi_v$, a line that runs in the north-south direction. Then $\mathcal{A}_{C_u,C_v}$ is precisely the collection of circles formed as intersections $\Pi \cap \mathbb{S}^2$ as Π ranges over all 2-planes in $\mathbb{E}^3$ that contain the line $\ell_{u,v}$. Notice that the circles in the coaxial family $\mathcal{A}_{C_u,C_v}$ project orthogonally to the family of lines in $\mathbb{C}$ that pass through the common point q, the intersection of the vertical line $\ell_{u,v}$ with the equatorial plane $\mathbb{C}$. This explains the position of the projections of A_1 and A_2 in Fig. 14(a). In this set up, local maxima

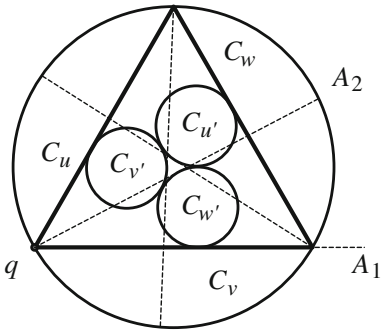

Fig. 15 The view of a critical *circle* realization for $\mathcal{O}(1, b, 1, 1)$ from above the north pole, with C_u, C_v, and C_w centered on the equator

for $d(t)$ occur when the three circles corresponding to u', v' and w' are all centered on the equator. This occurs once when the flow μ_t is hyperbolic or parabolic, and periodically with two different local maximum values as the flow pushes the circle across the equator when elliptic. By shifting the origin, we may assume that a local maximum occurs at time $t = 0$ so that the circles $C_{u'}(0)$, $C_{v'}(0)$, and $C_{w'}(0)$ are centered on the equator, and, without loss of generality, we may assume that the flow is oriented so that $C_{w'}(t)$ is centered in the upper hemisphere for initial positive values of t. Under these normalizations $d(t) = d(-t)$ and $C_{w'}(-t) = I_O(C_{w'}(t))$ for all t, where O is the equator. The resulting realizations of the Ma–Schlenker octahedra of the form $\mathcal{O}(a, b, c, d)$ have order three rotational symmetry about the axis through the north and south poles. We should comment that a realization built in this manner will not be a circle packing. To obtain a packing these will need to be Möbius flowed using a hyperbolic flow from the north toward the south pole.

As an example, we construct a critical circle packing for the Ma–Schlenker octahedron $\mathcal{O}(1, b, 1, 1)$ where $b > 1$ and $d(\tau) = 1$. Choose C_u, C_v, and C_w to have equal radii of $\pi/3$ so that the three circles are mutually tangent and project orthogonally to an equilateral triangle inscribed in the unit circle, as in Fig. 15. Choose $A_1 = C_v$ and A_2 so that the circles $C_{u'}(t)$, $C_{v'}(t)$, and $C_{w'}(t)$ are disjoint except at two values $t = \pm\tau$ of the flow variable, when the circles are mutually tangent. Automatically, $d(t)$ must take on its isolated minimum values at $t = \pm\tau$ where $d(\pm\tau) = 1$, with $d(t) > 1$ for $t \neq \pm\tau$. To obtain a critical Ma–Schlenker c-octahedron, apply the hyperbolic Möbius flow from the north toward the south pole whose flow lines are the meridianal circles until the centers of C_u, C_v, and C_w lie on a latitude L and those of $C_{u'}(\tau)$, $C_{v'}(\tau)$, and $C_{w'}(\tau)$ lie on a latitude L' of equal radii, L centered on the south pole and L' on the north. The resulting realization is a circle packing and therefore a critical Ma–Schlenker c-octahedron.

References

1. Bowers, P.L., Hurdal, M.K.: Planar conformal mappings of piecewise flat surfaces. In: Hege, H.-C., Polthier, K. (eds.) Visualization and Mathematics III, Chapter 1, pp. 3–34. Springer, Berlin (2003)
2. Bowers, P.L., Stephenson, K.: Uniformizing dessins and Belyĭ maps via circle packing. Mem. Am. Math. Soc. **170**(805), 1–97 (2004)

3. Guo, R.: Local rigidity of inversive distance circle packing. Trans. Am. Math. Soc. **363**(9), 4757–4776 (2011)
4. Luo, F.: Rigidity of polyhedral surfaces, III. Geom. Topol. **15**(4), 2299–2319 (2011)
5. Ma, J., Schlenker, J.-M.: Non-rigidity of spherical inversive distance circle packings. Discrete Comput. Geom. **47**(3), 610–617 (2012)